JACS
JOURNAL OF THE AMERICAN CHEMICAL SOCIETY

Communication

pubs.acs.org/JACS

Three-Dimensional Metal-Catecholate Frameworks and Their Ultrahigh Proton Conductivity

Nhung T. T. Nguyen,[†,‡] Hiroyasu Furukawa,[†] Felipe Gándara,[§] Christopher A. Trickett,[†] Hyung Mo Jeong,[†] Kyle E. Cordova,[†,‡] and Omar M. Yaghi*[,†,∥]

[†]Department of Chemistry, University of California—Berkeley; Materials Sciences Division, Lawrence Berkeley National Laboratory; Kavli Energy NanoSciences Institute at Berkeley; and Global Science Institute at Berkeley, Berkeley, California 94720, United States

[‡]Center for Molecular and NanoArchitecture (MANAR), Vietnam National University—Ho Chi Minh City, Ho Chi Minh City 721337, Vietnam

[§]Department of New Architectures in Materials Chemistry, Instituto de Ciencia de Materiales de Madrid, Consejo Superior de Investigaciones Científicas, Madrid 28049, Spain

[∥]King Abdulaziz City of Science and Technology, Riyadh 11442, Saudi Arabia

Supporting Information

ABSTRACT: A series of three-dimensional (3D) extended metal catecholates (M-CATs) was synthesized by combining the appropriate metal salt and the hexatopic catecholate linker, H_6THO (THO^{6-} = triphenylene-2,3,6,7,10,11-hexakis(olate)) to give Fe(THO)·Fe(SO_4)($DMA)_3$, Fe-CAT-5, Ti(THO)·$(DMA)_2$, Ti-CAT-5, and V(THO)·$(DMA)_2$, V-CAT-5 (where DMA = dimethylammonium). Their structures are based on the **srs** topology and are either a 2-fold interpenetrated (Fe-CAT-5 and Ti-CAT-5) or noninterpenetrated (V-CAT-5) porous anionic framework. These examples are among the first catecholate-based 3D frameworks. The single crystal X-ray diffraction structure of the Fe-CAT-5 shows bound sulfate ligands with DMA guests residing in the pores as counterions, and thus ideally suited for proton conductivity. Accordingly, Fe-CAT-5 exhibits ultrahigh proton conductivity (5.0×10^{-2} S cm^{-1}) at 98% relative humidity (RH) and 25 °C. The coexistence of sulfate and DMA ions within the pores play an important role in proton conductivity as also evidenced by the lower conductivity values found for Ti-CAT-5 (8.2×10^{-4} S cm^{-1} at 98% RH and 25 °C), whose structure only contained DMA guests.

Although, a large number of metal—organic frameworks (MOFs) are known,[1] surprisingly only five are based on the catechol linking functionality with two having 3D framework structures.[2,3] Usually, it is a challenge to find suitable conditions under which a new linking functionality would yield an extended porous structure in crystalline form, thus impeding progress in expanding the realm of frameworks available for study. Here, we report the synthesis and characterization of crystalline 3D anionic frameworks of metal-catecholates (M-CATs) constructed from H_6THO (THO^{6-} = triphenylene-2,3,6,7,10,11-hexakis(olate)) and Fe(II,III), Ti(IV), and V(IV), termed Fe-CAT-5, Ti-CAT-5, and V-CAT-5, respectively, Figure 1. We find that the first member of this series, Fe-CAT-5, exhibits ultrahigh proton conductivity rivaling that of the best MOFs[4−6] and comparable to Nafion.[7] We believe that since the linkage type in

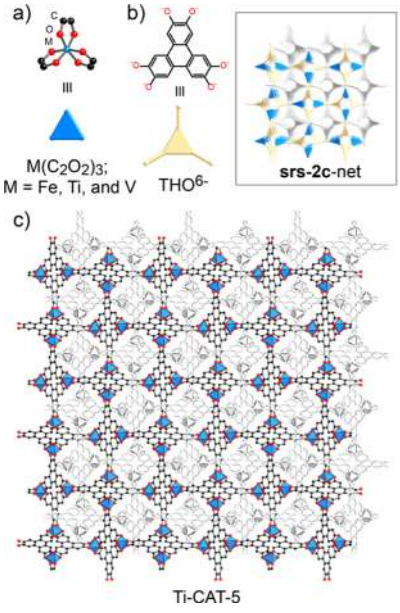

Figure 1. Fe-, Ti-, and V-CAT-5 are constructed from triangular $M(C_2O_2)_3$ single metal secondary building units (a) linked together through triangluar THO^{6-} organic linkers (b). The resulting structure is an interpenetrated **srs-2c** framework. It is noted that V-CAT-5 forms a noninterpenetrated **srs** framework. Inset: Simplified representation of **srs-2c** topology. Atom colors: M, blue; C, black; O, red; second interpenetrated framework, gray; all H atoms are omitted for clarity.

MOFs determines, to a large extent, their architectural, physical, and chemical properties, our success here in making the catecholate frameworks expands the scope of this chemistry and offers the promise of accessing improved or new properties.

All members of this series were synthesized using a *N*,*N*-dimethylformamide (DMF) solution of the appropriate metal salt with the H_6THO linker in the presence of tetrabutylammonium salt (Sections S1 and S2, Supporting Information). As a

Received: October 20, 2015
Published: November 23, 2015

DOI: 10.1021/jacs.5b10999
J. Am. Chem. Soc. 2015, 137, 15394−15397

representative example, Fe-CAT-5 was prepared by dissolving iron(II) sulfate, H_6THO, tetrabutylammonium nitrate, and amylamine in a solvent mixture of DMF/water/methanol (10/1/1, *v*/*v*, respectively) in a Teflon vessel, which was then sealed and placed in a stainless steel Parr autoclave. The autoclave was placed in an oven preheated at 180 °C under autogenerated pressure for 48 h (Section S2, SI). Black, truncated octahedral-shaped crystals, of suitable size for single crystal X-ray diffraction (SXRD) analysis, were isolated in 36% yield based on the linker. Although, crystals of appropriate quality for SXRD could not be obtained for Ti-CAT-5 and V-CAT-5 (Section S3, SI), their framework structures were determined to be similar to Fe-CAT-5 using powder X-ray diffraction (PXRD) and the charge flipping method.

The single crystal structure of Fe-CAT-5 was solved in the cubic space group, $Pa\bar{3}$ (No. 205), with a lattice parameter of a = 17.7594(7) Å (Table S1, Section S4, SI). Each organic linker is coordinated to three, crystallographically equivalent, octahedral iron atoms, Fe(THO), to generate a 3D architecture with **srs** topology (Figure 1). Due to a relatively large pore space, interpenetration by a second framework was observed, in which the center-to-center distance between two THO linkers from neighboring nets is ca. 6.6 Å. Additionally, these two frameworks were found to be connected through an $Fe_2(SO_4)_2(H_2O)_2$ cluster, whereby each Fe atom in this cluster adopts an octahedral geometry as a result of three μ_2-O atoms from the organic linkers, two bridging SO_4^{2-} anions, and one H_2O ligand (Figure 2). The Fe−O bond distance is slightly longer in the

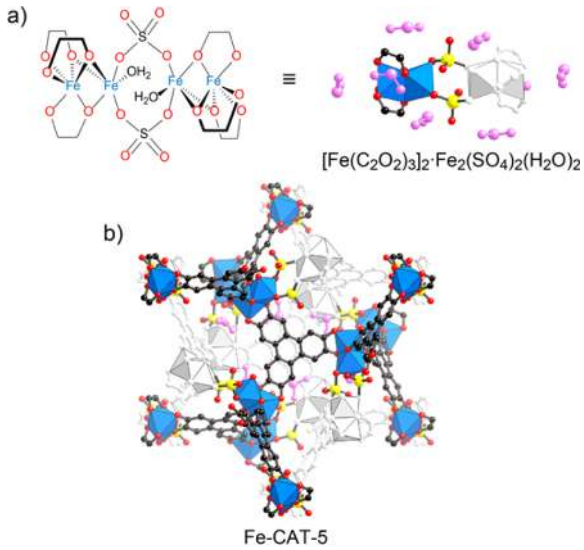

Figure 2. Illustration of the bridging $Fe_2(SO_4)_2(H_2O)_2$ cluster (a) surrounded by DMA ions, which connects the two interpenetrated **srs** frameworks in Fe-CAT-5 (b). Atom colors: Fe, blue and gray polyhedra; C, black; O, red; S, yellow; DMA ion, pink; all H atoms are omitted for clarity.

$Fe_2(SO_4)_2(H_2O)_2$ bridging cluster (2.138 Å) than in the Fe(THO) unit comprising the frameworks (1.998 Å), indicating that the Fe atoms of the bridging cluster are weakly bound to the organic linkers. Indeed, the coordinated Fe atoms to the oxygen atoms of catecholate linkers observed in Fe-CAT-5 is similar to that observed in $Na_5\{Ho[benzene\text{-}1,2,4,5\text{-}tetrakis(olate)]_2\}\cdot 7H_2O$.[2b]

Based on SXRD analysis alone, the oxidation and protonation states of the Fe atoms and THO linker,[8] respectively, could not be fully resolved. Therefore, a combination of Fourier-transform infrared spectroscopy (FT-IR), proton nuclear magnetic resonance spectroscopy (^{1}H NMR), Mössbauer spectroscopy, and elemental microanalysis were utilized to determine a plausible chemical formula for Fe-CAT-5. Prior to these analyses, guest-free, activated materials for all members of this series were prepared by washing thoroughly with DMF and anhydrous acetonitrile before evacuation (10^{-4} Torr) at room temperature for 24 h (Section S2, SI). The crystallinity of the activated materials was subsequently confirmed by PXRD analyses (Section S5, SI). The protonation state of the THO linker was first examined by FT-IR, in which there were no significant peaks observed in the spectrum that could be attributable to O−H stretching vibrations. Accordingly, the THO linker was presumed to be fully deprotonated (Section S6, SI). Furthermore, the presence of DMA cations in an integrated ratio of 3:1 with the THO linker was established by ^{1}H NMR spectroscopy on an acid digested sample of activated Fe-CAT-5 (Section S7, SI). Taking into account these results along with the SXRD analysis, it is evident that the Fe atoms in Fe-CAT-5 must have oxidation states of both 2+ and 3+. As expected, Mössbauer spectroscopy measurements confirmed the existence of both Fe^{2+} and Fe^{3+} in a ratio of nearly 1:1 (Section S8, SI). Although the distribution of these iron atoms in different oxidation states cannot be specifically assigned within the structure, elemental analysis data (calcd, C, 43.05; H, 4.25; N, 7.06; S, 4.43%; found, C, 43.28; H, 4.81; N, 7.25; S, 5.00%) further supported the chemical formula of Fe-CAT-5 as $Fe(THO)\cdot Fe(SO_4)(DMA)_3(DMF)_{0.65}H_2O$ (Section S2, SI).

PXRD analysis was performed on microcrystalline powders of Ti-CAT-5 and V-CAT-5 to elucidate the structural features of these frameworks. First, the diffraction patterns for both members were indexed in primitive cubic systems ($P2_13$ and $P4_332$ for Ti-CAT-5 and V-CAT-5, respectively) with the resulting unit cell parameters being similar to Fe-CAT-5 (a = 17.986 and 17.795 Å for Ti-CAT-5 and V-CAT-5, respectively) (Section S4, SI). A full Pawley refinement was then performed to extract the refined unit cell parameters and integrated intensities, from which the charge-flipping algorithm was employed to obtain electron density maps of Ti-CAT-5 and V-CAT-5 (Figures S5 and S6, SI).[9] The positions of the metal ions and THO linkers were clearly observed in the electron density maps, indicating a doubly interpenetrated and a noninterpenetrated **srs** framework for Ti-CAT-5 and V-CAT-5, respectively (Figures S5 and S6, SI). Accordingly, computational models of both structures were constructed, and full pattern refinements were performed (Rietveld method)[10] against the experimental powder patterns resulting in converging refinements and low residual values (a = 17.996 Å, R_p = 5.66%, R_{wp} = 8.05% for Ti-CAT-5; a = 17.765(8) Å, R_p = 5.85%, R_{wp} = 9.03% for V-CAT-5) (Figure 3 and Table S2, SI). It is noted that additional electron density was observed in the pores of both structures, which were attributed to DMA cations. These molecules were included in the computational models and refined with rigid body constraints.

A similar procedure as that described for Fe-CAT-5 was undertaken to formulate Ti-CAT-5 and V-CAT-5. From the absence of O−H stretching modes in the FT-IR spectra of both members, it was presumed that the H_6THO linker is fully deprotonated (Section S6, SI). When considering that the molar ratio of metal ion (Ti and V) and organic linker in the crystal structure is unity, it is likely that countercations are accommodated within the framework to compensate the negative charge from the linker. Indeed, the ^{1}H NMR spectra

DOI: 10.1021/jacs.5b10999
J. Am. Chem. Soc. 2015, 137, 15394−15397

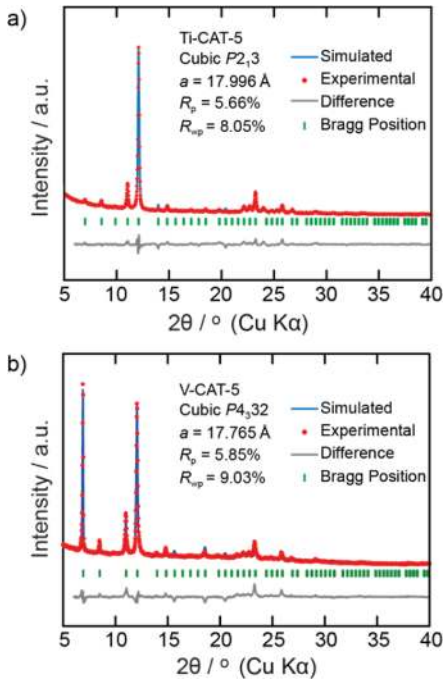

Figure 3. Experimental (red) and refined (blue) PXRD patterns of Ti-CAT-5 (a) and V-CAT-5 (b) after Rietveld refinement. The difference plot is provided in gray. The reflection positions are represented by the green tick marks.

of the acid-digested samples displayed the presence of two DMA cations per THO linker (Section S7, SI). Consequently, the chemical formula of Ti-CAT-5 and V-CAT-5 must be described as $Ti(THO)\cdot(DMA)_2$ and $V(THO)\cdot(DMA)_2$, respectively, where Ti and V have the same oxidation state of 4+. Elemental analysis for Ti-CAT-5 (calcd, C, 56.16; H, 3.99; N, 6.13%; found, C, 56.02; H, 4.19; N, 6.05%) and for V-CAT-5 (calcd, C, 52.25; H, 4.77; N, 8.08%; found, C, 51.75; H, 4.90; N, 7.68%) further confirmed these formulations (Section S2, SI).

To evaluate the architectural stability and porosity of all members of this series, thermal gravimetric analysis (TGA) and N_2 isotherms at 77 K were performed on activated samples. The TGA curves displayed no significant weight loss up to 200 °C, indicating high thermal stability and that successful and proper activation was achieved for Fe-CAT-5, Ti-CAT-5, and V-CAT-5 (Section S9, SI). N_2 gas adsorption isotherms at 77 K were then performed (Section S10, SI). The Brunauer–Emmett–Teller (BET) surface areas for Ti-CAT-5 and V-CAT-5 were calculated to be 450 and 725 $m^2\ g^{-1}$, respectively (Section S10, SI). The N_2 adsorption isotherm at 77 K for Fe-CAT-5 revealed no significant uptake (BET < 10 $m^2\ g^{-1}$). In spite of this, the water sorption isotherm at room temperature for Fe-CAT-5 demonstrated a high uptake capacity around 30 mol mol^{-1} (235 $cm^3\ g^{-1}$) at P/P_0 = 0.9, which was similar to that found also for Ti-CAT-5 (Section S11, SI). Finally, both Fe-CAT-5 and Ti-CAT-5 are stable in air after 24 h of exposure, as evidenced by PXRD analysis (Section S12, SI). In contrast, the crystallinity of V-CAT-5 was slightly diminished after only 3 h of exposure to an open-air environment (Section S12, SI).

The high water uptake capacity at elevated RH and the presence of DMA cations within the pores points to the possible utility of Fe-CAT-5 and Ti-CAT-5 as proton conducting materials (Section S4 and S11, SI). Accordingly, the proton conductivity properties of these two structures were investigated by subjecting the appropriate pelleted samples to ac impedance spectroscopy measurements under varying RH (50–98%) at 25 °C (Section S13, SI). The Nyquist plots for Fe-CAT-5 and Ti-CAT-5 confirm that the proton conductivity values of these materials were strongly dependent on RH, with increasing conductivity observed when the RH was increased as well (Section S13, SI). This led to maximum proton conductivity values of 5.0×10^{-2} and 8.2×10^{-4} S cm^{-1} for Fe-CAT-5 and Ti-CAT-5, respectively, being reached at 98% RH and 25 °C (Figure 4). Lower values, 2.1×10^{-5} and 4.3×10^{-6} S cm^{-1} for Fe-CAT-5

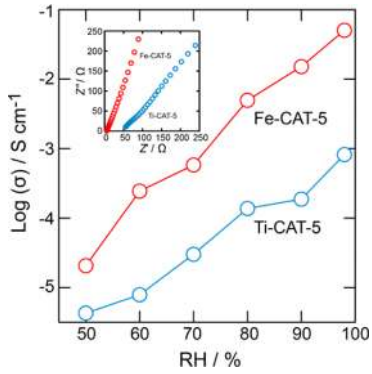

Figure 4. Dependence of proton conductivity on relative humidity for Fe-CAT-5 and Ti-CAT-5. Inset: Nyquist plots at 98% RH and 25 °C.

and Ti-CAT-5, respectively, were obtained when the RH was decreased to 50% (Figure 4). It is noted that Fe-CAT-5 exhibited a proton conductivity value of 2.4×10^{-4} S cm^{-1} at 60% RH, which is over 1 order of magnitude higher than Ti-CAT-5 under identical conditions (Figure 4). Furthermore, the proton conductivity of Fe-CAT-5 is 60 times higher than Ti-CAT-5 under 98% RH and at 25 °C (Figure 4). Indeed, this value is comparable to that of Nafion as well as several of the highest performing MOF materials under similar conditions (Table 1).

Table 1. Proton Conductivity (σ) at 25 °C and 98% RH and Activation Energy (E_a) Values for Nafion and Several of the Highest Performing MOFs

material	σ (S cm^{-1})[a]	E_a (eV)
Fe-CAT-5	5.0×10^{-2}	0.24
Ti-CAT-5	8.2×10^{-4}	0.43
$(NH_4)_2(adp)[Zn_2(ox)_3]\cdot 3H_2O$[b,c]	8.0×10^{-3}	0.63
$[(DMA)_3(SO_4)]_2[Zn_2(ox)_3]$[c]	4.2×10^{-2}	n/a
Nafion	1.0×10^{-1}	0.14–0.41

[a]98% RH, 25 °C. [b]adp = adipate. [c]ox = oxalate.

PXRD analysis was performed in order to prove the structural integrity of both samples after ac impedance measurements. As expected, the crystallinity of both Fe-CAT-5 and Ti-CAT-5 was retained (Section S13, SI).

The dependency of the proton conductivity on temperature was investigated by performing ac impedance measurements on pelleted samples of Fe-CAT-5 and Ti-CAT-5 over a temperature range of 15–65 °C at 95% RH. The Arrhenius plot establishes the fact that the proton conductivity of both materials increases with increasing temperature (Section S13, SI). The calculated activation energies, as determined by linear regression analysis, were found to be 0.24 and 0.43 eV for Fe-CAT-5 and Ti-CAT-5, respectively (Table 1). These activation energies indicate that the proton conduction behaviors occur through a Grotthuss

DOI: 10.1021/jacs.5b10999
J. Am. Chem. Soc. 2015, 137, 15394–15397

mechanism, in which protons are hopping through a hydrogen-bonded network.[11]

It is noted that Fe-CAT-5 exhibits significantly higher proton conductivity than Ti-CAT-5 over the entire RH range measured, even though the latter structure effectively adsorbs more water molecules per formula unit (22 water molecules at $P/P_0 = 0.6$) than Fe-CAT-5 (7.7 water molecules at $P/P_0 = 0.6$) as evidenced by the water sorption isotherms (Section S11, SI). This observation implies that, at least comparatively, the proton conductivity in these materials is not simply governed by the water concentration, but rather, it is influenced by other ionic species within the pores (i.e., DMA and sulfate ions). Furthermore, by considering the fact that Fe-CAT-5 has a larger amount of both DMA and sulfate ions per formula unit (3 DMA and 2 sulfates for Fe-CAT-5, and only 2 DMA for Ti-CAT-5), it is deduced that the sulfate and DMA ions in Fe-CAT-5 play an important role in achieving higher proton conductivities over the entire RH range examined.

■ ASSOCIATED CONTENT

Supporting Information

The Supporting Information is available free of charge on the ACS Publications website at DOI: 10.1021/jacs.5b10999.

Synthesis and full characterization specifics, single crystal X-ray analysis data for Fe-CAT-5, PXRD analysis, including refinement, computational modeling, and charge-flipping method details for Ti-CAT-5 and V-CAT-5, and proton conductivity experimental methods and data (PDF)
Fe-CAT-5 CIF (CIF)
Ti-CAT-5 CIF (CIF)
V-CAT-5 CIF (CIF)

■ AUTHOR INFORMATION

Corresponding Author

*yaghi@berkeley.edu

Notes

The authors declare no competing financial interest.

■ ACKNOWLEDGMENTS

We acknowledge Dr. T. Chantarojsiri and Prof. C. Chang (UC Berkeley) for assistance on performing Mössbauer spectroscopy measurements and Dr. R. Chatterjee (LBNL) for useful discussion on characterization of our samples. Drs. S. Teat and K. Gagnon are acknowledged for the synchrotron X-ray diffraction data acquisition support at the beamline 11.3.1 at Advanced Light Source, Lawrence Berkeley National Laboratory. The synthesis and characterization were supported by BASF SE (Ludwigshafen, Germany) and U.S. Department of Defense, Defense Threat Reduction Agency (HDTRA 1-12-1-0053), respectively. Work performed at the Advanced Light Source is supported by the Director, Office of Science, Office of Basic Energy Sciences, of the U.S. Department of Energy under Contract No. DE-AC02−05CH11231. N.T.T.N. and K.E.C. acknowledge financial support for the design and elaboration of this project from Vietnam National University−Ho Chi Minh (No. A2015-50-01-HĐ-KHCN) and the United States Office of Naval Research Global: Naval International Cooperative Opportunities in Science and Technology Program (No. N62909-15-1N056). F.G. acknowledges financial support from Fundación General CSIC (Programa ComFuturo).

■ REFERENCES

(1) (a) Furukawa, H.; Cordova, K. E.; O'Keeffe, M.; Yaghi, O. M. *Science* **2013**, *341*, 1230444. (b) Zhang, J.-P.; Zhang, Y.-B.; Lin, J.-B.; Chen, X.-M. *Chem. Rev.* **2012**, *112*, 1001. (c) Phan, A.; Doonan, C. J.; Uribe-Romo, F. J.; Knobler, C. B.; O'Keeffe, M.; Yaghi, O. M. *Acc. Chem. Res.* **2010**, *43*, 58. (d) Côté, A. P.; Shimizu, G. K. H. *Coord. Chem. Rev.* **2003**, *245*, 49.

(2) (a) $[M^{II}_2(DHBQ)_3](NBu_4)_2$ (where M = Mn, Fe, Co, Ni, Zn, Cd; DHBQ = benzene-1,2,4,5-tetrakis(olate), $C_6H_2O_4^{2-}$; NBu_4 = tetrabutylammonium): Abrahams, B. F.; Hudson, T. A.; McCormick, L. J.; Robson, R. *Cryst. Growth Des.* **2011**, *11*, 2717. (b) $Na_5[Ho(DHBQ)_2]$: Nakabayashi, K.; Ohkoshi, S. *Inorg. Chem.* **2009**, *48*, 8647. (c) Mn(DHBQ): Morikawa, S.; Yamada, T.; Kitagawa, H. *Chem. Lett.* **2009**, *38*, 654. (d) $Ln_2(DHBQ)_3$ and $Ln_2(CAN)_3$ (where Ln = Y, La, Ce, Gd, Yb, Ln, Th; CAN = benzene-3,6-dichloro-1,2,4,5-tetrakis(olate)): Abrahams, B. F.; Coleiro, J.; Ha, K.; Hoskins, B. F.; Orchard, S. D.; Robson, R. *J. Chem. Soc., Dalton Trans.* **2002**, 1586.

(3) $\{[M_6(THO)_4(H_2O)_{12}]\cdot[M_3(THO)(H_2O)_{12}]\}_4$, (where M = Co, Ni; THO^{6-} = triphenylene-2,3,6,7,10,11-hexakis(olate)): Hmadeh, M.; Lu, Z.; Liu, Z.; Gándara, F.; Furukawa, H.; Wan, S.; Augustyn, V.; Chang, R.; Liao, L.; Zhou, F.; Perre, E.; Ozolins, V.; Suenaga, K.; Duan, X.; Dunn, B.; Yamamto, Y.; Terasaki, O.; Yaghi, O. M. *Chem. Mater.* **2012**, *24*, 3511.

(4) Sadakiyo, M.; Yamada, T.; Honda, K.; Matsui, H.; Kitagawa, H. *J. Am. Chem. Soc.* **2014**, *136*, 7701.

(5) Nagarkar, S. S.; Unni, S. M.; Sharma, A.; Kurungot, S.; Ghosh, S. K. *Angew. Chem., Int. Ed.* **2014**, *53*, 2638.

(6) (a) Taylor, J. M.; Dekura, S.; Ikeda, R.; Kitagawa, H. *Chem. Mater.* **2015**, *27*, 2286. (b) Kim, S. R.; Dawson, K. W.; Gelfand, B. S.; Taylor, J. M.; Shimizu, G. K. H. *J. Am. Chem. Soc.* **2013**, *135*, 963. (c) Panda, T.; Kundu, T.; Banerjee, R. *Chem. Commun.* **2013**, *49*, 6197. (d) Li, S.-L.; Xu, Q. *Energy Environ. Sci.* **2013**, *6*, 1656. (e) Jeong, N. C.; Samanta, B.; Lee, C. Y.; Farha, O. K.; Hupp, J. T. *J. Am. Chem. Soc.* **2012**, *134*, 51. (f) Horike, S.; Umeyama, D.; Inukai, M.; Itakura, T.; Kitagawa, S. *J. Am. Chem. Soc.* **2012**, *134*, 7612. (g) Sadakiyo, M.; Ōkawa, H.; Shigematsu, A.; Ohba, M.; Yamada, T.; Kitagawa, H. *J. Am. Chem. Soc.* **2012**, *134*, 5472. (h) Ponomareva, V. G.; Kovalenko; Chupakhin, A. P.; Dybtsev, D. N.; Shutova, E. S.; Fedin, V. P. *J. Am. Chem. Soc.* **2012**, *134*, 15640. (i) Pardo, E.; Train, C.; Gontard, G.; Boubekeur, K.; Fabelo, O.; Liu, H.; Dkhil, B.; Lloret, F.; Nakagawa, K.; Tokoro, H.; Ohkoshi, S.; Verdaguer, M. *J. Am. Chem. Soc.* **2011**, *133*, 15328. (j) Shigematsu, A.; Yamada, T.; Kitagawa, H. *J. Am. Chem. Soc.* **2011**, *133*, 2034. (k) Sahoo, S. H.; Kundu, T.; Banerjee, R. *J. Am. Chem. Soc.* **2011**, *133*, 17950. (l) Umeyama, D.; Horike, S.; Inukai, M.; Hijikata, Y.; Kitagawa, S. *Angew. Chem., Int. Ed.* **2011**, *50*, 11706. (m) Yoon, M.; Suh, K.; Kim, H.; Kim, Y.; Selvapalam, N.; Kim, K. *Angew. Chem.* **2011**, *123*, 8016. (n) Bureekaew, S.; Horike, S.; Higuchi, M.; Mizuno, M.; Kawamura, T.; Tanaka, D.; Yanai, N.; Kitagawa, S. *Nat. Mater.* **2009**, *8*, 831. (o) Ōkawa, H.; Shigematsu, A.; Sadakiyo, M.; Miyagawa, T.; Yoneda, K.; Ohba, M.; Kitagawa, H. *J. Am. Chem. Soc.* **2009**, *131*, 13516. (p) Sadakiyo, M.; Yamada, T.; Kitagawa, H. *J. Am. Chem. Soc.* **2009**, *131*, 9906. (q) Kitagawa, H.; Nagao, Y.; Fujishima, M.; Ikeda, R.; Kanda, S. *Inorg. Chem. Commun.* **2003**, *6*, 346.

(7) Slade, S.; Campbell, S. A.; Ralph, T. R.; Walsh, F. C. *J. Electrochem. Soc.* **2002**, *149*, A1556.

(8) Barthram, A. M.; Cleary, R. L.; Kowallick, R.; Ward, M. D. *Chem. Commun.* **1998**, 2695.

(9) (a) Palatinus, L.; Chapuis, G. *J. Appl. Crystallogr.* **2007**, *40*, 786. (b) Oszlanyi, G.; Suto, A. *Acta Crystallogr., Sect. A: Found. Crystallogr.* **2008**, *64*, 123. (c) Gándara, F.; Uribe-Romo, F. J.; Britt, D. K.; Furukawa, H.; Lei, L.; Cheng, R.; Duan, X.; O'Keeffe, M.; Yaghi, O. M. *Chem. - Eur. J.* **2012**, *18*, 10595.

(10) Young, R. A. *The Rietveld Method*; IUCr Book Serials, Oxford University Press: Oxford, U.K., 1993.

(11) (a) Yoon, M.; Suh, K.; Natarajan, S.; Kim, K. *Angew. Chem., Int. Ed.* **2013**, *52*, 2688. (b) Yamada, T.; Otsubo, K.; Makiura, R.; Kitagawa, H. *Chem. Soc. Rev.* **2013**, *42*, 6655.

DOI: 10.1021/jacs.5b10999
J. Am. Chem. Soc. 2015, 137, 15394−15397